Hierarchical titania nanostructures prepared with focused ion beam-assisted anodisation of titanium in an aqueous electrolyte

Pradeep K. Yadav · Patrick Lemoine · Graham Dale ·
Jeremy W. J. Hamilton · Patrick S. M. Dunlop ·
John A. Byrne · Pascal Mailley · Colin Boxall

Abstract Titania nanostructures have been prepared by anodisation in aqueous solution assisted by focused ion beam (FIB) milling. The structures formed are bi-periodic, a disordered "native" nanotube array, with characteristics similar to those formed by the standard anodisation process and an ordered array of tubes with larger diameters, guided by the positioning of the FIB concave pits. Low kV EDX analysis shows implanted Ga in FIB-treated titanium which is efficiently removed by the anodisation process. Following thermal annealing, the FIB-treated regions also crystallise to the same anatase phase as the native regions. This result is in stark contrast to previous FIB-assisted anodisation studies which only produced nanostructured arrays of native dimensions. This singularity is discussed in terms of the stable FIB-induced crystalline defects which, in an aqueous electrolyte, can result in the growth of a weaker barrier layer and larger tubes. This novel process gave hexagonal and square arrays with tailored cross-sectional dimensions and therefore has potential for the synthesis of novel meta-materials.

P. K. Yadav · P. Lemoine (✉) · G. Dale ·
J. W. J. Hamilton · P. S. M. Dunlop · J. A. Byrne
Nanotechnology and Integrated Bioengineering Center,
University of Ulster, Jordanstown, Shore Road,
Newtownabbey BT37 0QB, UK
e-mail: p.lemoine@ulster.ac.uk

P. Mailley
LETI-DTBS-SBSC, 17 rue des martyrs,
38054 Grenoble Cedex 9, France

C. Boxall
Engineering Department, Lancaster University,
Lancaster LA1 4YW, UK

1 Introduction

Anodic metal oxide films have been developed for many years as barrier layers. However, in specific electrolyte conditions, they can lead to self-organised nanostructures. Earlier work focused on porous anodic alumina, for generating nanotemplates [1] but quickly moved to titania, an electro-active, photo-active and biocompatible semiconductor with a wide range of applications. Indeed in the presence of fluorine ions, the anodic oxidation of titanium results in the formation of a self-organised array of nanotubes. These materials have generated much interest in water photo-electrolysis [2–4], gas sensing [5–7], solar cells [8–10] and biomedical implants [11]. The main progress to date has been in preparing titania arrays with longer tubes (several 100 μm) and better regularity, mainly by using two steps anodisation procedures and non-aqueous electrolytes such as ethylene glycol [12].

More recently, further improvements in order and regularity of the titania tube arrays have been achieved by directly pre-patterning the metal substrate using focused ion beam (FIB) milling [13, 14] prior to anodisation in an ethylene glycol electrolyte. This method provides means of obtaining structures other than the hexagonal close-pack array obtained by the self-organising process, hence widening the scope for applications of these nanostructured materials. However, the tubes formed by this process have similar diameter that those prepared without FIB milling, henceforth termed native, as previously observed for FIB-assisted anodisation of aluminium [15–17].

In the present study, FIB pre-patterning is also used albeit followed by anodisation in an aqueous electrolyte. The key novelty of this method is that it produces bi-periodic nanostructures, a disordered native nanotube array, with characteristics similar to those formed by the native anodisation process and an ordered array of tubes with larger diameters, controlled by the positioning of the FIB concave pits and by the ion dose. These characteristics increase the versatility and applicability of these titania nanostructures to meta-materials and photonic crystal applications.

2 Experimental

Ti plates (99.6 % purity, Advent Ltd.) were sonicated in iso-propanol and de-ionised (DI) water and dried in a nitrogen stream. This investigation follows from earlier work on the effect of mechanical polishing on the formation of titania nanotubes [18]. For the present study, the polishing recipe was modified to minimise damage and increase smoothness (R_a roughness value, measured by AFM microscopy, decreasing from 95 to 5 nm and specific surface area difference from 18.5 to 0.3 %). The main outcome of this introductory enquiry on the effect of polishing, shown in the supplementary material (figure S1 and S2), is that the native nanotubes are similar for the as-received and polished metal plates. Hence, the present study focuses on the FIB-assisted anodisation of unpolished titanium.

For both the native and FIB-assisted anodisation processes, we used a weakly acidic electrolyte solution (pH 7) consisting of 1 M Na_2SO_4 and 0.13 M NaF solution with DI water (Sigma-Aldrich, purity, ≥99 %). The anodisation was carried out as previously described [19] at room temperature under a constant voltage of 20 V for 30 min, with a platinum reference electrode as a cathode and the titanium metal sheet as anode [20, 21]. Previous studies have shown that for such a dilute solution, a two-electrode set-up with a Pt reference is adequate [22].

The FIB nanopatterning was carried out with a FEI Quanta 3D dual beam system operated with a 30 kV Ga^+ beam and beam current of 30 and 300 pA, measured with a Faraday cup positioned on the sample stage. The patterns were either square or hexagonal, with size ranging from 1×1 to 20×20 μm^2 and spacing ranging from 125 to 1,000 nm. The dwell times per point were multi-pass and varied from ∼0.3 to 2.3 s, giving Ga^+ dose varying from 1.0×10^8 to 1.7×10^9 Ga/point. The depth and diameter of the milled holes were controlled within the patterning software by the beam current and dwell time, as the ion beam had a Gaussian cross section. They were measured by atomic force microscopy (AFM), as discussed below

giving pit diameter varying from 33 to 170 nm and Ga doses varying from 2.8×10^{18} to 1.5×10^{19} Ga ion/cm^2. The FIB was also used at low current (30 pA) to produce cross sections.

The FIB pre-patterned and anodised surfaces were imaged by scanning electron microscopy (SEM) at 20 kV, in secondary electron mode, with the SEM beam of the Quanta 3D system or alternatively with a Hitachi S3200N SEM system. EDX analyses of FIB-treated regions were performed with a Link ISIS spectrometer with 5 kV electron energy. The corresponding Kanaya electron ranges [23] are 265 and 280 nm for Ti and TiO$_2$, respectively. This indicates that such low kV EDX analysis is relatively surface sensitive to detect compositional changes in sub-surface regions following either FIB irradiation or anodisation.

Tapping atomic force microscopy (TAFM) images were obtained with a Veeco DI 3200 system using a Si mono-beam cantilever (40 N/m) at 1 Hz at high tapping set point, to minimise sample damage. However, repeated imaging of the anodic titania nanotubes was delicate as these are high aspect ratio hard surfaces which can produce significant tip blunting. This was monitored by imaging periodically a Nioprobestandard (Electron Microscopy Sciences) to detect eventual change in tip apex geometry. The surfaces of the FIB pits on Ti were easier to image, being of lower aspect ratio, and with local slope smaller than the AFM tip half-apex angle, the AFM tip artefact was negligible in this case. These AFM measurements gave FIB pit diameters and depths of 33–170 and 20–100 nm, respectively. Finally, an ISA LabRam confocal Raman microscope equipped with a Helium–Neon ($\lambda = 633$ nm) laser source was used to identify the crystalline phases in the anodised sample following a slow thermal annealing (2 h at 500 °C with 1 °C/min ramping gradients).

3 Results

In Fig. 1, we present SEM micrographs for the FIB-assisted process for anion beam current of 30 pA for various pattern spacings and dwell times. The samples are displayed before and after anodisation. The titania nanotube structures consist of a background of disordered native nanotubes, with apparent characteristics similar to those formed by the standard anodisation process and an ordered array of tubes with larger diameters, guided by the positioning of the FIB concave pits. One observed a threshold milled depth/time (∼12 nm/0.3 s for this 30 pA ion current) below which no super-tubes can be formed. Others have also found in a FIB-assisted anodisation study on alumina [15] that the pores could only grow above a given trigger depth, ∼15 nm. These FIB irradiation thresholds
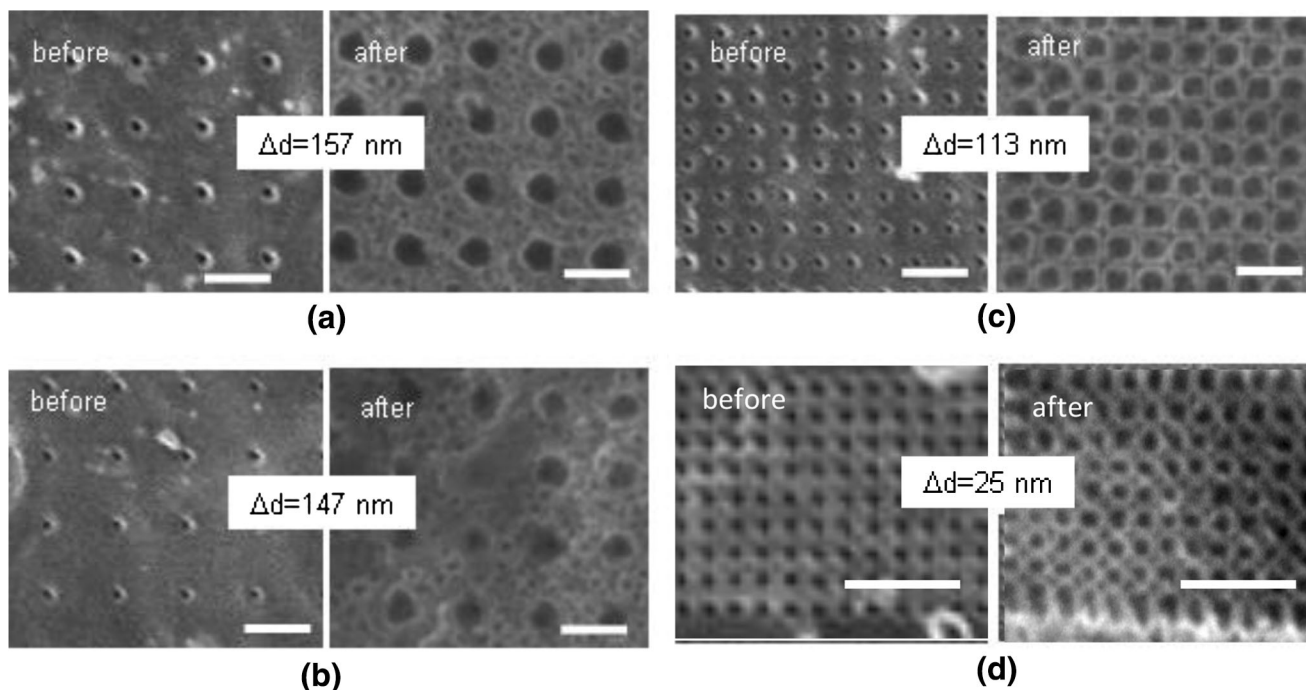
Fig. 1 FIB-assisted anodisation of titanium, low FIB current ($\sim$30 pA): SEM micrographs, at the same magnification, showing the surface morphology before and after anodisation. The FIB spacing (s) and dwell time (t) are as follows: **a** $s = 500$ nm and $t = 2.34$ s, **b** $s = 500$ nm and $t = 0.44$ s, **c** $s = 250$ nm and $t = 0.55$ s and **d** $s = 125$ nm and $t = 0.55$ s. The Δd values (in nm) represent the difference in diameter between the FIB-guided tubes and the original FIB pit. The *space bars* represent 500 nm

for the formation of TiO_2 tubes or Al_2O_3 pores may correspond to a critical change in topography, composition or structure of the pristine material.

The larger nanotubes seen on the anodised samples, produced at the locations of the FIB pits, can be characterised by Δd, reported in Fig. 1 which represents the difference between their diameter and the diameter of the original FIB pit. For large FIB spacings (500 nm), the Δd values are clearly larger than d_o; the diameter of the native tubes ($d_0 = 101 \pm 22$ nm, see supplementary information S1) and the FIB-assisted process yields "super-tubes" (i.e. larger than native tubes). Obviously, the diameter of the FIB pit contributes to the diameter of the final "super-tube". We believe, however, that this geometric effect does not explain the formation of these "super-tubes" as the diameter increase after anodisation ($\Delta d = +150$ nm to $+233$ nm) is much larger than the diameter of the native tubes (101 nm). When the spacing is intermediate ($s = 250$ nm in Fig. 1c), the super-tubes are constrained and adopt a square cross section, as seen in previous FIB-guided anodisation studies [13, 14, 16, 17]. Finally, when the FIB spacing becomes close to the diameter of the native tube ($s = 125$ nm in Fig. 1d), the two processes yield similar structures. One also notices
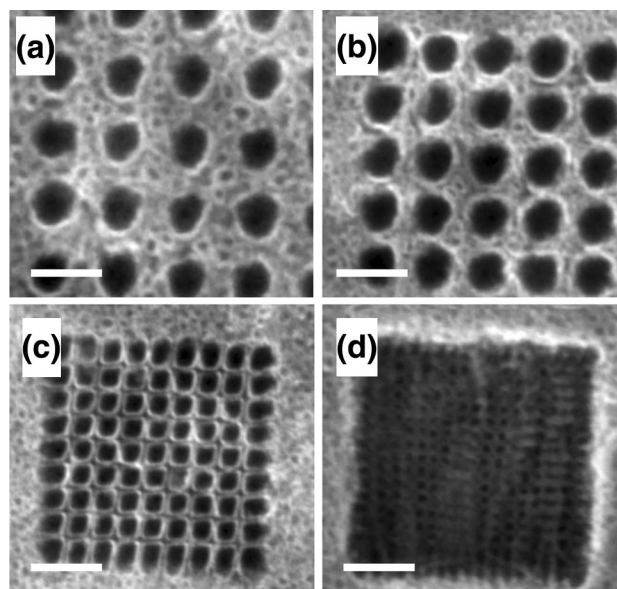

Fig. 2 FIB-assisted anodisation of titanium, high FIB current ($\sim$300 pA): the SEM micrographs are at the same magnification and show the surface morphology after anodisation. The FIB spacing (s) and dwell time (t) are as follows: **a** $s = 500$ nm and $t = 0.27$ s, **b** $s = 500$ nm and $t = 0.88$ s, **c** $s = 250$ nm and $t = 0.27$ s and **d** $s = 125$ nm and $t = 0.31$ s. The *space bars* represent 500 nm

that, on the edge of the array, the constraint is only from the half plane and results in larger super-tubes (Fig. 1d).

In Fig. 2, similar results are presented for an ion beam current of 300 pA. Here, the images only display the surfaces post-anodisation. Again, FIB-assisted anodisation results in super-tube structures. For large spacings (>125 nm), the super-tubes formed at 300 pA have larger dimensions ($d = 200$–350 nm) than those prepared at 30 pA, shown in Fig. 1 ($d = 200$–250 nm). AFM analysis of these super-tubes also showed a depth increase upon anodisation; for instance, for the super-tubes of Fig. 2a, the FIB pits were ~ 130 nm deep, whereas the corresponding super-tubes are ~ 300–400 nm deep. Here also, proximal tubes constrain their neighbours, with a relaxation of this constraint on the edge of the array (Fig. 2c).

Figure 3 shows the FIB-assisted anodisation for again a 300-pA FIB current but with larger spacing i.e. 1,000 nm. The surface morphology is shown both before and after anodisation. These large tubes ($d = 470$ nm, $\Delta d = 310$ nm) have native tubes ($d \sim 100$ nm) growing both between and inside them, as shown in the high magnification inset in Fig. 3b. Figure 4 shows EDX analysis at 5 kV of sample regions inside and outside FIB-treated regions, before and after anodisation. Clearly, the FIB treatment results in Ga incorporation, readily detectable for such low kV analysis. After anodisation, there is a presence of carbon (CK) and fluorine (FK peak) but the Ga content present in the original array has been removed, very probably driven out of the sample into the electrolyte and
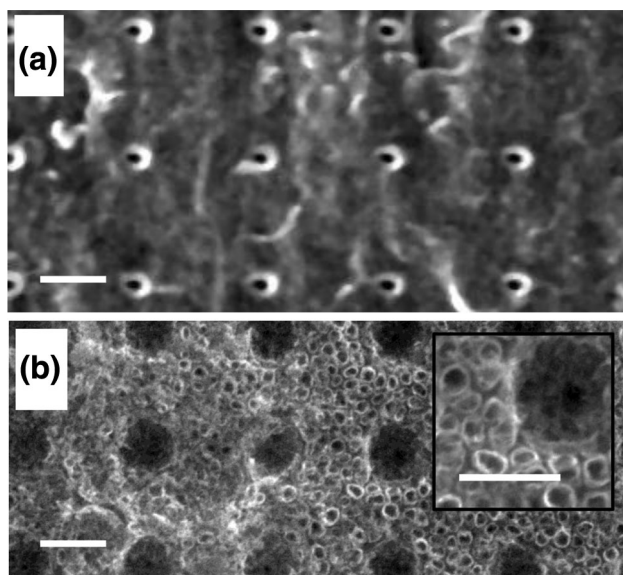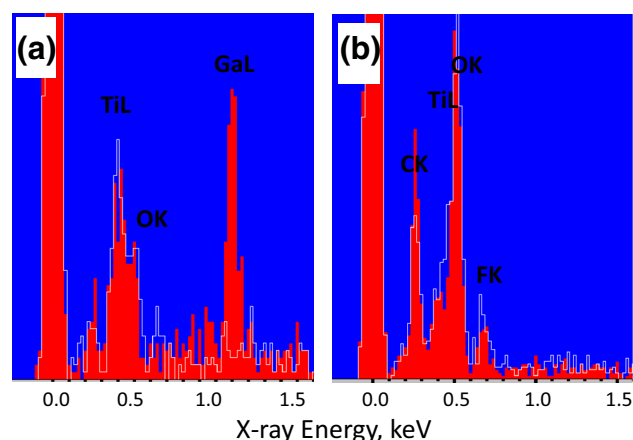

Fig. 4 EDX spectra of FIB-assisted titania nanotubes: the analyses were carried out in (*red*) and out (*white*) of the FIB-irradiated area before (**a**) and after (**b**) anodisation. The spectra were acquired at 5 kV

towards the cathode during anodisation. Moreover, after anodisation, the spectra inside and outside the FIB-treated area are very similar. Hence, the effect of FIB milling on the super-tube formation process is not compositional; it is either structural or topographical.

Figure 5 shows super-tubes based on square and hexagonal FIB trigger arrangements resulting in cross sections with approximately square and hexagonal geometries for
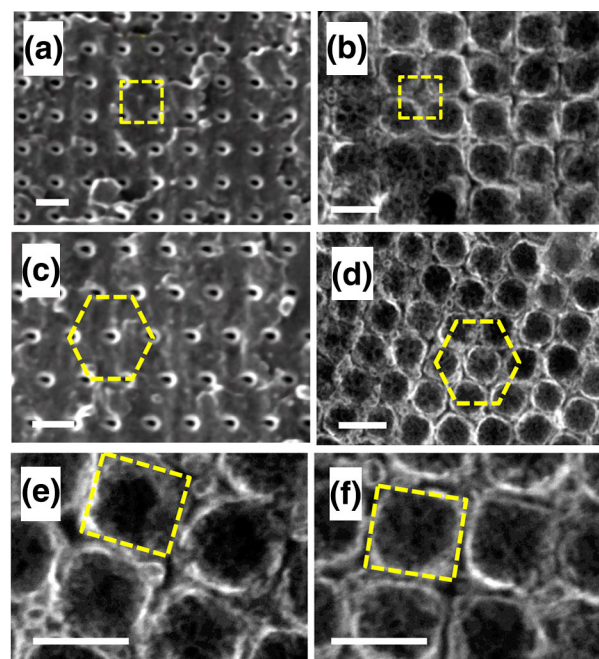

Fig. 3 FIB-assisted anodisation of titanium, high FIB current (~ 300 pA) for large spacing (1,000 nm): the SEM micrographs are at the same magnification and show the surface morphology before (**a**) and after (**b**) anodisation. The *inset* in **b** shows a higher magnification of a super-tube. The *space bars* represent 500 nm

Fig. 5 *Square* and *hexagonal arrays* of super-tubes prepared with FIB nanopatterning. *Square array* before (**a**) and after (**b**) anodisation, *hexagonal array* before (**c**) and after (**d**). Higher magnification micrographs of the *anodised square array* before (**e**) and after (**f**) thermal annealing. The *space bars* represent 500 nm
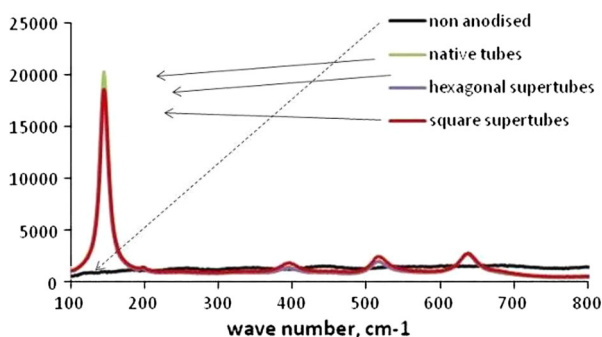
Fig. 6 Confocal Raman spectra for the various anodic titania samples

the two respective FIB patterns. A slow thermal annealing resulted in no noticeable changes in the morphology of the super-tube array as seen on the SEM micrographs. Confocal Raman analysis of these arrays, shown in Fig. 6, indicates that before annealing, the spectrum has few characteristic features indicative of amorphous titania. After annealing, all sample regions (native tubes, square and hexagonal super-tubes) display very similar Raman features, with the characteristic anatase peak at around 150 cm^{-1}. This indicates that the super-tubes formed by this FIB nanopatterning process thermally anneal into a structure similar to that of annealed native tubes. Resisting annealing is a perquisite for most applications which rely on the use of crystalline titania.

Figure 7 shows the result of FIB sectioning experiments performed at 30 pA with cuts performed at 90° and 45° incidence angles. In this case, there is probably some degree of damage and re-deposition of the milled material around the cross sections. However, one can see that the super-tubes are around 300–500 nm deep, in accordance with the AFM measurement previously mentioned. One also notices that the native tubes are much deeper ($\sim$900 nm).

4 Discussion

Some of the results presented here have been observed in previous FIB-guided anodisation of alumina [16, 17, 24–26] and titania [13, 14] nanostructures, namely that the FIB patterns yield ordered arrays of tubes/pores of both square and hexagonal geometries. Moreover, for intermediate FIB spacings, the growing tubes/pores are constrained and adopt square or hexagonal cross-sectional areas.

In some of these earlier investigations [14, 17], when using smaller FIB spacings, two types of pores/tubes were grown simultaneously; those grown on the FIB pits reaching their final diameter, i.e. the diameter obtained in the native anodisation process (i.e. without FIB irradiation)

and those starting from intermediate positions, constrained by the surrounding larger features and consequently of smaller diameter. A similar self-compensating effect was observed for anodic titania tube arrays seeded by closely spaced nanoimprints [27]. By contrast, the bi-periodic tubes grown in the present study are observed for large spacing (Fig. 3), with the tubes positioned on the FIB pits having a larger diameter than those prepared by the native process. This represents a striking departure from the FIB-guided anodisation results published to date. This contrasting finding is analysed, starting with the established description of the native growth process and discussing its validity for FIB-guided anodisations.

Generally, the growth of anodic nanostructures can be described as a three-stage growth sequence:

1. The formation of a continuous barrier layer. The thickness of this oxide film is a function of the anodisation voltage, electrolyte composition and pH. However, its growth is driven by ionic transport and facilitated by point defects, such as oxygen vacancies and metallic interstitials, as described in the point defect model [28]. Hence, new defects created by FIB irradiation could modify this barrier layer.

2. The growth of characteristic features (pores/tubes), initiated at local defect sites, often identified as penetration paths [29] and accelerated by local field enhancement caused by the topography of the interfaces at these defect sites. Hence, the FIB pit geometry may modify the dynamics of tube formation. In addition, analytical models [30, 31] show that the feature diameter relates directly to the barrier oxide thickness. Hence, new defects created by FIB irradiation could influence the final diameter of the tubes.

3. The competitive self-organisation of these features, essentially due to their fast lateral growth rate and the high surface density of initial defect sites. The bulk defect density in rutile varies from 1 to $60 \times 10^7 \mu m^{-3}$ [32]. The equivalent surface defect densities are 4.6–$71.1 \times 10^4 \mu m^{-2}$, much larger than the native tube density ($\sim$57 μm^{-2} in figure S1a). FIB spacing obviously impacts on this competitive process, as observed in previous FIB-guided anodisation studies [13, 14, 16, 17].

That FIB irradiation can introduce new point defects and even bring amorphisation is well documented [33, 34]. In the case of titanium, the increase in point defect concentration can be significant for a number of reasons. The masses of Ga (48 g/mol) and Ti (61 g/mol) are such that, in an elastic collision between the gallium ion projectile and a titanium target atom, there is a 98.4 % energy transfer to the Ti target atom. In addition, gallium is poorly soluble in the titanium lattice according to the Hume-Rothery rule

Fig. 7 Tilted SEM micrographs of a FIB sectioned across the super-tube array. The FIB trenches permit to view the native tubes and FIB tubes in cross section. The FIB tubes are ∼300 nm deep (**a**, **b**), whereas the native tubes are ∼900 nm deep (**b**). A lower magnification micrograph is shown in (**c**). The *space bar* represents 1,000 nm
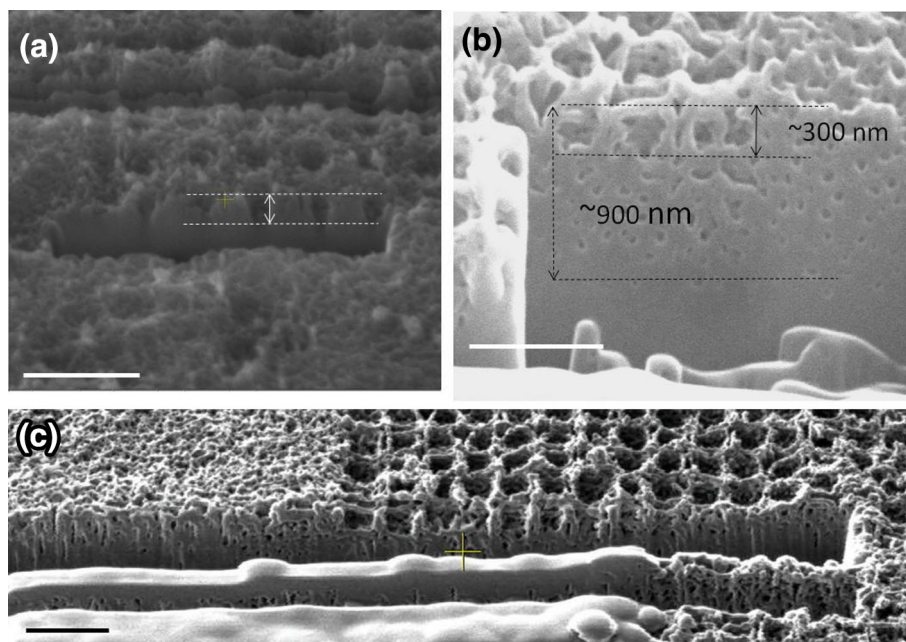
[35] (large difference in atomic radius, valence, electronegativity and crystal structure). Indeed, binary phase diagrams show that Ti and Ga segregate into a bi-phasic intermetallic compound [36]. Hence, gallium implantation would result in significant disturbances into the Ti network and new point defects, following anodisation and gallium removal. A number of studies suggest that these defects do not fully self-anneal and, therefore, can contribute to the anodisation process. For instance, one investigation by Schmuki's group [37] showed that focused ion beam (FIB) milling using Si ions on a Si substrate results in the formation of porous silicon after electrochemical treatment. In that case, the FIB treatment does not modify the topography of the Si wafer and TRIM calculations [38] show that the triggers for pore formation are stable crystalline atomic defects and interstitial FIB atoms. In another study [39], crystalline defects are again implanted with an ion beam, in this case Ge ions in Ge single crystals, and the stability of these defects is demonstrated using nanoindentation. Similar results were obtained on cobalt nanoparticles [40].

The absence of such large structures in previous FIB-guided anodisation studies must be due to the different preparation conditions used in the present study. The first notable difference is the use of an aqueous electrolyte. Its increased conductivity (10× higher than in the previous FIB-guided anodisation of titania [13, 14]) and larger H^+ ion concentration would boost the chemical dissolution of titania. In that sense, in an aqueous electrolyte, the FIB-induced defects can be more efficiently utilised in the anodisation reactions. The water content also results in a loss of regularity when compared to organic electrolytes, as previously observed [13]. This has been interpreted as

originating from current transients and PH burst at the bottom of the pore tips [41]. The other difference is the larger FIB dose used in this study (2×10^{18}– 1.5×10^{19} Ga ion/cm^2) when compared to previous ones (8×10^{17} Ga ion/cm^2 [13, 14] and 2×10^{13} Ga ion/cm^2 [17, 18]). The effect of these larger doses on the diameter of the titania nanotubes grown on the FIB pits can be seen clearly in Fig. 8. The diameter increase also becomes larger after the ion dose is increased (from 3.7×10^{18} to 1.5×10^{19} Ga$^+$/cm^2, Δd increases by 59 %), and this hinting that the growth of these "super-tubes" is not a geometric effect but results from the ion dose.

As discussed above, the resulting larger defect density and deeper damage profile could lead to a thicker barrier layer and larger diameter tubes. Indeed, the anodisation of titania under UV/visible illumination also results in larger
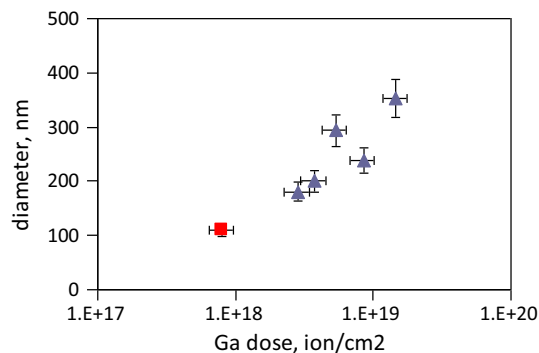

Fig. 8 Effect of Ga ion dose (ion/cm^2) on FIB tube diameter, for the measurements taken in the present study (*blue triangles*) and previous FIB-assisted anodisation of titanium (Refs. [13, 14], *red square*)

tubes, attributed by the authors to the optical generation of electron–hole pairs in the band gap, i.e. defect states, which results in larger anodisation currents [42].

To conclude, the work presented here permitted to prepare non-closed packed super-tube anodic titania structures (see Fig. 3). The method is interesting as it has applications for the fabrication of photonic and phononic crystals, which are often based on such non-closed packed structures, for endoscopic applications [43] and broadband sound blockage [44]. In addition, such hierarchical surfaces can find applications as super-hydrophilic coatings [45]. More broadly, the possibility of using ion beams to seed point defects in valve metals offers exciting possibilities to prepare a wider [1] range of anodised oxide nanostructures.

5 Conclusions

We used FIB pre-patterning to prepare ordered arrays of anodic titania nanotubes. The surfaces were anodised in a Na_2SO_4/NaF aqueous solution. This results in both native titania tubes (~ 100 nm diameter randomly located) and larger tubes (~ 200–470 nm diameter on the FIB pits). EDX analysis and Raman analysis show that the native and super-tube structures have similar composition and anneal to the same anatase crystal structure. In addition, this technique permitted to prepare non-close packed square and hexagonal arrangements of tubes, despite with lower regularity than those previously prepared with organic electrolytes. Hence, the production of these super-tubes is possibly due to the generation of crystalline defects in Ti resulting from the ion implantation.

References

1. G.E. Thompson, Thin Solid Films **297**, 192 (1997)
2. G.K. Mor, K. Shankar, O.K. Varghese, C.A. Grimes, J. Mater. Res. **19**, 2989 (2004)
3. G.K. Mor, K. Shankar, M. Paulose, O.K. Varghese, C.A. Grimes, Nano Lett. **5**, 191 (2005)
4. O.K. Varghese, M. Paulose, K. Shankar, G.K. Mor, C.A. Grimes, J. Nanosci. Nanotechnol. **5**, 1158 (2005)
5. U. Kirner, K.D. Schierbaum, W. Gopel, Sens. Actuators B **1**, 103 (1990)
6. C.V.G. Reddy, S.V. Manorama, J. Electrochem. Soc. **147**, 390 (2000)
7. Y. Shimizu, N. Kuwano, T. Hyodo, M. Egashira, Sens. Actuators B **83**, 195 (2002)
8. B. O'Regan, M. Gratzel, Nature **353**, 737 (1991)
9. M. Gratzel, Nature **414**, 338 (2001)
10. R. Tenne, C.N.R. Rao, Philos. Trans. R. Soc. A **362**, 2099 (2004)
11. D. Kowalski, D. Kim, P. Schmuki, Nano Today **8**, 235 (2013)
12. G. Zhang, H. Huang, Y. Liu, L. Zhou, Appl. Catal. B **90**, 262 (2009)
13. B. Chen, K. Lu, Z. Tian, Langmuir **27**(2), 800 (2011)
14. B. Chen, K. Lu, Z. Tian, J. Mater. Chem. **21**, 8835 (2011)
15. A.P. Robinson, G. Burnell, M. Hu, J.L. MacManus-Driscoll, Appl. Phys. Lett. **91**, 143123 (2007)
16. B. Chen, K. Lu, Z. Tian, Electrochim. Acta **56**, 435 (2010)
17. Z.P. Tian, K. Lu, B. Chen, Nanotechnology **21**, 405301 (2010)
18. G.R. Dale, J.W.J. Hamilton, P.S.M. Dunlop, P. Lemoine, J.A. Byrne, J. Nanosci. Nanotech. **9**, 4215 (2009)
19. G. Dale, Electrochemical growth Titania nanotubes: characterisation and electrochemistry, PhD Dissertation, University of Ulster, Jordanstown, 2009
20. G.K. Mor, O.K. Varghese, M. Paulose, K. Shankar, C.A. Grimes, Sol. Energ. Mat. Sol. C. **90**, 2011 (2006)
21. G. Patermarakis, K. Moussoutzanis, J. Electrochem. Soc. **142**, 737 (1995)
22. C. Longo, A.F. Nogueira, M.A. DePaoli, J. Phys. Chem. B **106**, 5925 (2002)
23. K. Kanaya, S. Okayama, J. Phys. D Appl. Phys. **5**, 43 (1972)
24. C.Y. Liu, A. Datta, Y.L. Wang, Appl. Phys. Lett. **78**(1), 120 (2001)
25. N.W. Liu, A. Datta, C.Y. Liu, Y.L. Wang, Appl. Phys. Lett. **82**(8), 1281 (2003)
26. A.P. Robinson, G. Burnell, M. Hu, J.L.M. Driscoll, Appl. Phys. Lett. **91**, 143123 (2007)
27. J. Choi, R.B. Wehrspohn, J. Lee, U. Gosele, Electrochim. Acta **49**, 2645 (2004)
28. D.D. Macdonald, Electrochim. Acta **56**, 1761 (2011)
29. G.E. Thompson, R.C. Furneaux, G.C. Wood, Nature **272**(5652), 433 (1978)
30. V.P. Parkhutik, V.I. Shershulsky, J. Phys. D Appl. Phys. **25**, 1258 (1992)
31. S.K. Thamida, H.C. Chang, J. Appl. Phys. **12**(1), 240 (2002)
32. M.A. Henderson, Surf. Sci. **419**, 174 (1999)
33. A. Schilling, T. Adams, R.M. Bowman, J.M. Gregg, Nanotechnology **18**, 035301 (2007)
34. A.A. Tseng, Small **1**(10), 924 (2005)
35. "Hume-Rothery Rules", Van Nostrand's Scientific Encyclopedia, Wiley, 2002
36. J.E. Hatch, *Aluminium: properties and physical metallurgy* (American Society for Metals, Metals Park, 1998)
37. P. Schmuki, L.E. Erickson, D.J. Lockwood, J. Porous Mater. **7**, 233 (2000)
38. J.F. Ziegler, *The stopping and range of ions in matter*, vol. 2–6, (Pergamon Press, New York, 1977-1985)
39. D.J. Oliver, S. Ruffell, J.E. Bradby, J.S. Williams, M.V. Swain, P. Munroe, P.J. Simpson, Phys. Rev. B **80**, 115210 (2009)
40. D.J. Sprouster, R. Giulian, L.L. Araujo, P. Kluth, B. Johannessen, D.J. Cookson, G.J. Foran, M.C. Ridgway, J. Appl. Phys. **107**, 014313 (2010)
41. J.M. Macak, H. Tsuchiya, L. Taveira, S. Aldabergerova, P. Schmuki, Angew. Chem. Int. **44**, 7493 (2005)
42. Y.R. Smith, B. Sarma, S.K. Mohnaty, M. Misra, ACS Mater. Interfaces **4**, 5883 (2012)
43. J. Jung, L. Martin-Moreno, F.J. Garcia-Vidal, New J. Phys. **11**, 123013 (2009)
44. J. Christensen, L. Martín-Moreno, F.J. García-Vidal, Appl. Phys. Lett. **97**, 134106 (2010)
45. S. Song, L. Jing, S. Li, H. Fu, Y. Luan, Mater. Lett. **62**, 3503 (2008)